SAND2012-2307C

Thunderstorm Risks to Wind Farms

Hieu H. Nguyen,* Lance Manuel,* Matthew F. Barone,† Joshua A. Paquette†

As has been noted in recent times, thunderstorm downbursts can cause damage to multiple turbine units that are part of a wind farm because of the correlated wind inflow fields that the turbines are subjected to simultaneously. We extend a model for simulating downburst events and their effects on a single turbine unit to situations where turbines in a wind farm are subjected to correlated input from moving storms. The end-to-end simulation begins by first generating a storm touchdown and subsequent movement across or offset from a wind farm with a 6×4 rectilinear arrangement of 5-MW 90-m hub height turbines. The downburst model includes a slowly varying (non-turbulent) component and a turbulent component. The model is developed and calibrated based on Doppler radar data. Results show that different downbursts with different characteristics cause variable load uncertainty features to the wind farm.

I. INTRODUCTION

In previous work,[1] the authors developed and demonstrated the use of a simulation framework for studying the effect of a thunderstorm downburst on a single wind turbine. In the present study, this model and framework are extended to thunderstorm risks on an array of turbines in a wind farm. Because of the computational effort involved, high-performance computing resources are employed and two thunderstorm events with different track scenarios (with respect to the wind farm) are analyzed. Risks to the turbines resulting from their spatial distribution in the array and the correlated wind fields resulting from the simulated downbursts are discussed.

II. DOWNBURST WIND MODEL

The wind field model for thunderstorm downbursts may be represented by separately considering its non-turbulent and turbulent components. The non-turbulent wind velocity field is based on an analytical model[2,3,4] available in the literature. The radial velocity (U_r) and vertical velocity (U_z) components may be expressed as follows:

$$U_r(r,z,t) = \Pi(t)\, U_{rm}\, f(r,t)\, p(z,t) \tag{1}$$

$$U_z(r,z,t) = \Pi(t)\, U_{rm}\, g(r,t)\, q(z,t) \tag{2}$$

where

$f(r,t), p(z,t), g(r,t), q(z,t)$: model radial and vertical shaping functions.
$f(r,t)$: radial shaping function of radial wind velocity component.
$p(z,t)$: vertical shaping function of radial wind velocity component.
$g(r,t)$: radial shaping function of vertical wind velocity component.
$q(z,t)$: vertical shaping function of vertical wind velocity component.

$$f(r,t) = (r/r_m(t)) \exp\left[\left(1 - r^{2\alpha}/r_m^{2\alpha}(t)\right)/(2\alpha)\right] \tag{3}$$

$$p(z,t) = \frac{\exp\left(-c_1 z/z_m(t)\right) - \exp\left(-c_2 z/z_m(t)\right)}{\exp(-c_1) - \exp(-c_2)} \tag{4}$$

*Dept. of Civil, Architectural, and Environmental Engineering, University of Texas, Austin, Texas 78712
†Wind Power Technologies Department, Sandia National Laboratories, Albuquerque, NM 87185.
Sandia National Laboratories is a multi-program laboratory managed and operated by Sandia Corporation, a wholly owned subsidiary of Lockheed Martin Corporation, for the U.S. Department of Energys National Nuclear Security Administration under contract DE-AC04-94AL85000.

$$g(r,t) = \left(2 - r^{2\alpha}/r_m^{2\alpha}(t)\right)\exp\left[\left(1 - r^{2\alpha}/r_m^{2\alpha}(t)\right)/(2\alpha)\right] \quad (5)$$

$$q(z,t) = \frac{z_m(t)}{r_m(t)}\frac{\left[\exp\left(-c_1(z/z_m(t))\right) - 1\right]/c_1 - \left[\exp\left(-c_2(z/z_m(t))\right) - 1\right]/c_2}{\exp(-c_1) - \exp(-c_2)} \quad (6)$$

in which r refers to the radial distance from the moving storm center, z refers to the height AGL (above ground level), and t refers to time. Additionally, $\alpha = 2$, $c_1 = 0.22$, and $c_2 = 2.75$ are recommended for use with the model.[3] Also, $z_m(t) = z_{m0} - k_{zm}t$ is the time-dependent height to the maximum radial velocity, U_{rm}, where z_{m0} is the initial value of $z_m(t)$ and k_{zm} is the rate of change of $z_m(t)$ with time; $r_m(t) = r_{m0} + k_{rm}t$ is the time-dependent radial distance to U_{rm}, where r_{m0} is the initial value of $r_m(t)$ and k_{rm} is the rate of change of $r_m(t)$ with time; and $\Pi(t) = \sin(\pi t_d/t)$ is an assumed time-dependent storm intensity function[5] where t_d is the storm duration.

A turbulent wind field is superimposed on the non-turbulent field. It has been reported that downburst fluctuations are non-stationary in nature.[6,7,8] In this study, the nonstationarity is achieved using the amplitude modulation method as presented by Chen and Letchford[9] and summarized in Chay et al.[4] In this method, a correlated Gaussian stochastic process with zero mean and unit variance is first simulated using *standard* turbulence power spectral density functions and coherence functions. The turbulence spectrum is the IEC Kaimal spectrum. The turbulence standard deviation of $u-$, $v-$, $w-$component at any point in space is specified deterministically as a function of *time-varying mean wind speed*: $\sigma_u(x,y,z,t) = 0.14U_m(x,y,z,t)$; $\sigma_v(x,y,z,t) = 0.8\sigma_u(x,y,z,t)$; $\sigma_w(x,y,z,t) = 0.5\sigma_u(x,y,z,t)$ where $U_m(x,y,z,t)$ is the total mean wind speed at point (x,y,z) and time t. This introduces nonstationarity to the turbulence wind components.

III. DEFINITION OF DOWNBURST CASES

Downbursts from the NIMROD and JAWS[10,11] projects are studied. For the selected downburst model and its associated required parameters, unavailable information was either estimated using available information or this information on downburst parameters and functions was assumed. Table 1 summarizes parameters/functions for the two downbursts (selected from the NIMROD and JAWS projects) that are simulated.

Storm Parameters		NIMROD Yorkville	JAWS Average
U_{rm}	(m/s)	31	21
z_{m0}	(m)	130	80
k_{zm}	(m/s)	0.1	0.0
r_{m0}	(m)	940	1000
k_{rm}	(m/s)	0.5	1.0
t_d	(min)	20	16
U_{trans}	(m/s)	16	8
$U_{amb}(z = 90m)$	(m/s)	8	6

Table 1. Downburst Parameters.

IV. SCENARIO DESCRIPTION

Figure 1 shows a plan view of the scenario that depicts a wind farm and a generalized storm touchdown and track. The storm touchdown point (i.e., its center at $t = 0$) is assumed to be defined by $(x_0,\ y_0)$ relative to an inertial frame coordinate system defined at the center of the wind farm, where $x_0 = R_0\cos\theta_0$, $y_0 = R_0\sin\theta_0$. The storm is assumed to move in a straight line (its track) at a constant translation speed, U_{trans}. The angle, ϕ, which defines the direction of the storm translation relative to the X-axis of the inertial frame, is assumed to be constant. At time t, the storm's center is at $(x_t,\ y_t)$, where $x_t = R_0\cos\theta_0 + tU_{trans}\cos\phi$, $y_0 = R_0\sin\theta_0 + tU_{trans}\sin\phi$. Due to the nature of the problem, (R_0, θ_0, ϕ) can be random. The storm's outflow is assumed to be perturbed by the boundary layer environmental winds, $U_{amb}(z)$;[11] this ambient wind profile, $U_{amb}(z)$, is modeled by a power law, with a shear exponent of 0.2 in this study. The direction of ambient winds is assumed to be aligned with the X-axis of the inertial frame. The wind farm is assumed to have turbines arranged so that they are $8D = 1080$ meters apart in both longitudinal and lateral directions ($D = 126$ m is the rotor diameter of a wind turbine).

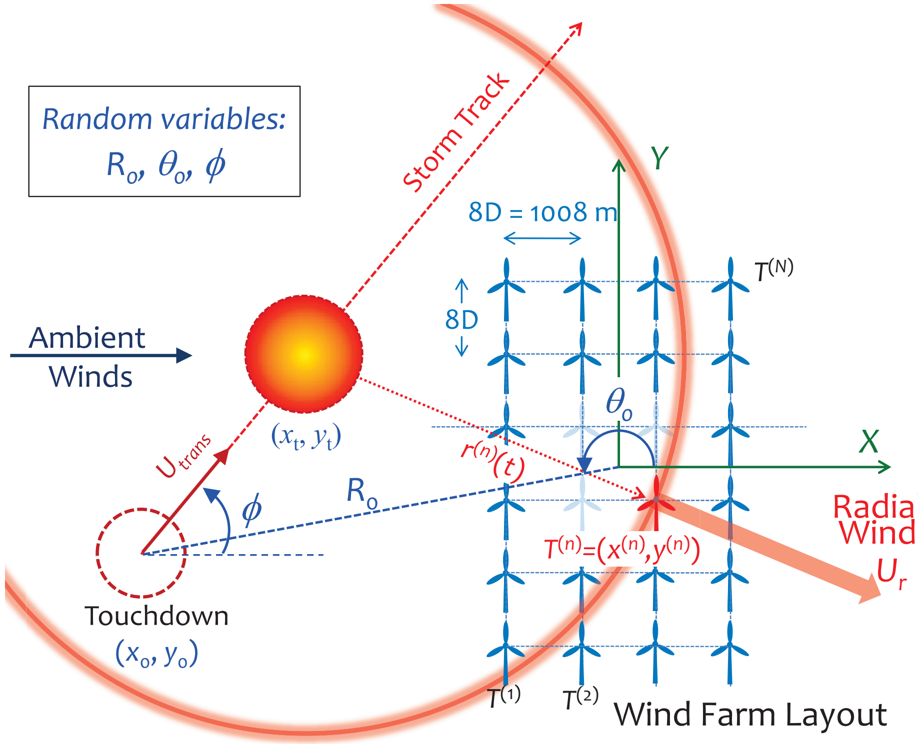

Figure 1. Plan View showing Turbines in Wind Farm in Path of Moving Storm.

V. THE 5MW WIND TURBINE MODEL

In this study, the NREL 5MW Onshore Baseline Wind Turbine model[12] is used in all the turbine response simulations. This model was originally developed to support concept studies aimed at assessing offshore wind turbine technology. The model describes a conventional three-bladed upwind variable-speed collective pitch-controlled turbine.

Properties/Dimensions	Values
Power Rating	5 MW
Rotor Type	Upwind/3 Blades
Rotor Diameter	126 (m)
Hub height	90 (m)
Cut-In, Rated, Cut-Out	3, 11.4, 25 (m/s)
Rated Rotor Speeds	12.1 (rpm)
Rotor Mass	110,000 (kg)
Nacelle Mass	240,000 (kg)
Tower Mass	347,460 (kg)

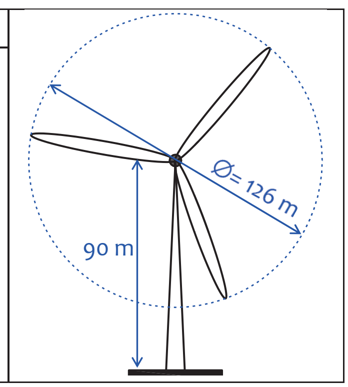

Table 2. Turbine Properties/Dimensions and Schematic Diagram.

Table 2 shows a schematic diagram of the 5-MW wind turbine and includes a summary of important turbine properties and dimensions. Figure 2 shows the pitch control, turbine rotor speed, and power curve

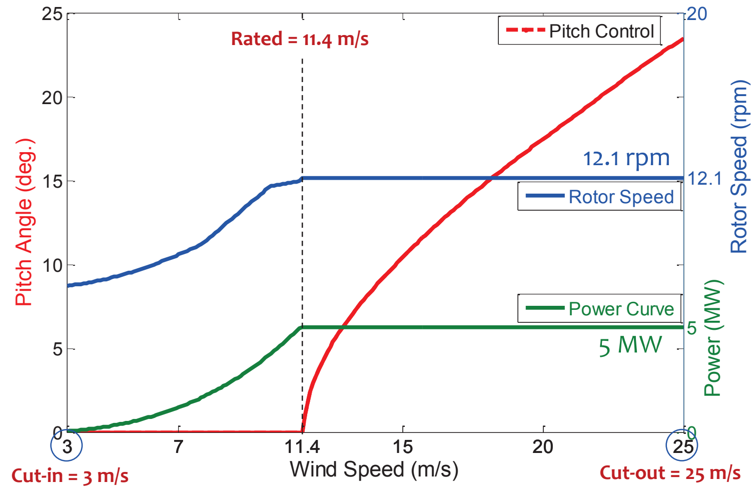

Figure 2. Pitch Control, Rotor Speed, and Power Curve.

as a function of the wind speed at hub height (90 m AGL).

VI. SIMULATION SETUP

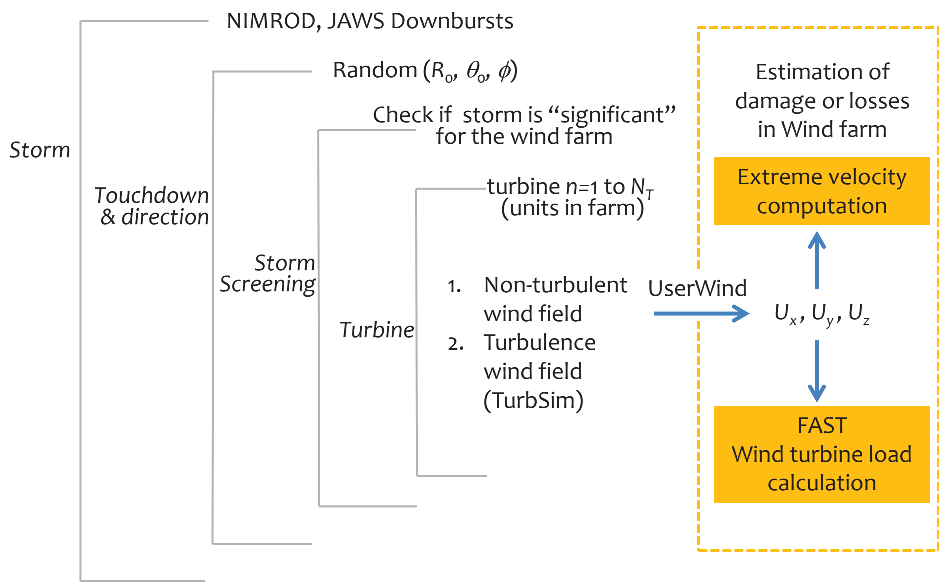

Figure 3. Integrated Assessment of Turbine Units in a Wind Farm for Simulated Thunderstorms.

Figure 3 shows a flow chart for the risk assessment of a wind farm in simulated thunderstorms. Storm's parameters are based on observed events in the NIMROD and JAWS[10, 11] project databases. In Monte Carlo simulations, the storm touchdown location, R_0, θ_0, and direction of translation, ϕ, are modeled as random variables (see Fig. 1). Realizations of these (i.e., R_0, θ_0, ϕ) will be checked for potential impact on the wind farm. If found to be significant (based on storm track); for each turbine unit, non-turbulent (mean) and turbulent wind fields will be generated separately. For the non-turbulent wind velocity field simulations, a 140 m $\times$ 140 m $\times$ 140 m grid with 10 m spacing and centered at the turbine hub is employed. The length of each numerical simulations depends on the duration of a storm. For example, in the JAWS Average downburst case whose duration, t_d, is 16 minutes, the simulation is run for the duration of 1,000 seconds with a time step, Δt, equal to 0.05 seconds. As a result, wind velocity time series are generated at $15^3 = 3375$ points on the grid described; each time series is comprised of 20,000 simulated wind velocity values.

The turbulent portion of the wind velocity field during the thunderstorm downburst uses the Fourier-based Veers method[13] over a rectangular grid describing a vertical plane; it uses the same temporal sampling and is simulated for the same duration as is used for the non-turbulent field. Turbulence is generated within the UserWind module of the FAST code[14] with the help from the turbulence simulator, TurbSim.[15] Taylor's frozen turbulence is assumed *at the single unit level* in order to obtain the turbulent component of the wind velocity at vertical grid points offset from $x = 0$. While the non-turbulent wind field is modeled as fully correlated, the turbulence coherence from turbine to turbine is neglected in this study. Here we make the assumption that turbulence coherence is negligible *between turbines* because the turbines are well-separated (the spacing is assumed to be $8D$ or 1,008 meters).

The full 4-D wind field (describing three orthogonal wind velocity components at discrete points in 3-D space and at discrete time instants) is imported into the aeroelastic simulation program, FAST[14] (using the UserWind module there). The equilibrium inflow model is used, which is a steady-state blade element momentum model. This is required in order to maintain numerical stability of the simulations over all wind speeds and the wide range of turbulent wind fields considered. However, this model is expected to be less accurate than other model choices in predicting dynamic loads. The effect of the wake model was explored in a previous work.[16]

Assumptions on yaw control are made as follows. When yaw control is required, the yaw rate is first set at the rate of non-turbulent wind direction change as long as this rate of change in wind direction is small; if/when this rate of change in wind direction becomes significant, this yaw rate is set to a maximum of 0.3 deg/sec.

In Monte Carlo simulations, the touchdown location, defined by (R_0, θ_0) values, and the storm translation direction, ϕ, are treated as random variables; they are assumed to be uniformly distributed. Effectively, the upper bound on R_0 is a function of t_d and $r_m(t)$, for $t = 0$ to t_d. The variable, ϕ is assumed to take values between -45 degrees and +45 degrees (see Fig. 1). The selected upper and lower bounds for all the uniformly distributed random variables (describing the storm touchdown point and the translation direction) are summarized in Table 3. Realizations of touchdown information and track direction (i.e., R_0, θ_0, ϕ) are assumed to have potential impact on the wind farm if they meet both of following requirements: (i) the distance from the end of the track to the center of the farm is less than $1.2L_{track}$, where $L_{track} = U_{trans} * t_d$ is the total length of the storm track; (ii) the distance from the center of the farm to the storm track is less than $0.5*8*D * \sqrt{nr^2 + nc^2}$, where nr and nc are the number of rows and columns of the farm, respectively. Further censoring is done after the simulation if necessary.

Table 3. Lower and Upper Bounds for the Uniformly Distributed Random Variables chosen in the Monte Carlo Simulations to Describe Touchdown Locations and Translation Directions

Downburst	R_0 (km)	θ_0 (deg)	ϕ (deg)
JAWS Average	(0, 9.21)	(0, 360)	(-45, 45)
NIMROD Yorkville	(0, 19.2)	(0, 360)	(-45, 45)

The DAKOTA software framework[17] is used for management of random sampling and simulation execution. The Latin hypercube sampling (LHS) option within DAKOTA is utilized, which offers efficiencies over the simpler Monte Carlo sampling method.[18] LHS is a stratified sampling method that divides the range of each sampled variable into intervals of equal probability, and one value is randomly selected from each interval with respect to the probability distribution within the interval. Compared with Monte Carlo sampling, LHS guarantees a more even sampling, and generally leads to better estimation of the output distribution with fewer samples. DAKOTA spawns a number of concurrent simulations on the available CPU cores, automatically creating a temporary work space and executing a user-defined job script. The job script populates the FAST/UserWind input file with the touchdown and track information, then executes FAST to loop over each of the turbine units. The FAST output is post-processed to extract extreme load values, which are then passed back to the DAKOTA process. DAKOTA saves the extreme load values for any load variable. DAKOTA also saves the touchdown variables for each simulation, which is useful should certain simulations require closer examination of the time series results at a later time.

The aero-elastic simulations are run on the Sandia Ebird computing cluster, a 5.5 teraflop Linux computing cluster. Ebird has 383 nodes, each with dual 3.6 GHz processors and 6 GB of RAM, giving a total of 766 available cores. The present results were obtained using 256 cores. This allows for simulation of 512 days of turbine operation in approximately 20 wall-clock hours. Use of a greater fraction of the cluster would result in faster simulation times. However, Ebird is a shared resource, so execution time must be balanced by queue wait time for jobs that request a relatively large number of cores. The 256 core job size was found to allow for efficient job throughput on Ebird. The FAST code was compiled within the Linux environment using the Intel Fortran90 compiler.

VII. NUMERICAL STUDIES

A. An Illustrative Turbine Response Simulation—JAWS "Average" Case

In this section, an illustrative single thunderstorm downburst and associated turbine response simulation is first discussed in some detail to highlight important characteristics of the flow fields and specific turbine response. The JAWS "average" downburst is chosen for these purposes. The storm touchdown point is chosen such that x_0 = -4 km, y_0 = 0, with respect to the turbine local coordinate system and the direction of translation of 15 deg. with respect to the ambient wind direction (see Fig. 4).

Although computations were carried out including the turbulent component as well, the figures showing time series that follow depict effects due to the non-turbulent wind field alone. Figure 4(a) shows a plan view of the moving downburst and the turbine for the selected downburst simulation. The centers of the circles describe the downburst locations at the beginning of the event and after 8 minutes.

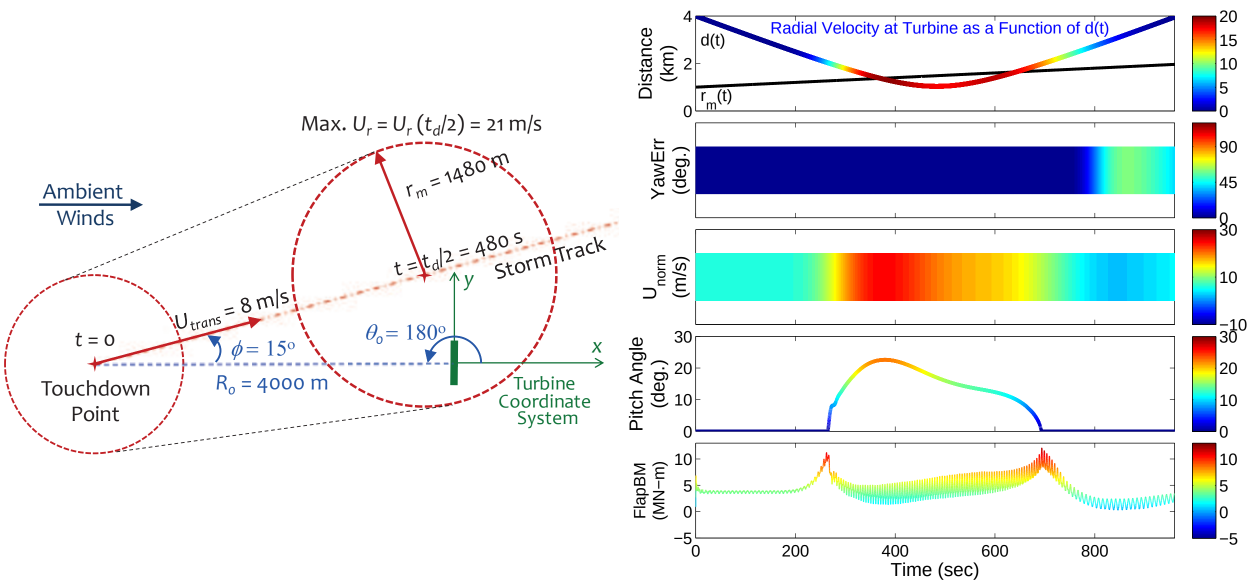

(a) Plan View showing Storm Track and Turbine.

(b) U_{amb} = 6 m/s; with Yaw Control.

Figure 4. JAWS "Average" Case. Note that $d(t)$ = distance from downburst to turbine); $r_m(t)$ = radius to maximum winds; U_{norm} = wind speed normal to the rotor plane; *Pitch Angle* = blade pitch angle; *FlapBM* = flapwise bending moment at blade root.

The upper panel of the figure shows the variation with time of the distance, $d(t)$, separating the center of the storm from the turbine; the radial distance from the storm center, $r_m(t)$, where the maximum velocity occurs; and the radial velocity at the turbine, shown with color variation, on the $d(t)$ plot. The storm-to-turbine distance, $d(t)$, indicates whether the storm is moving toward or away from the turbine. The radial distance to the maximum velocity is an indication of the changing size (i.e., spatial extent) of the storm. The plots of $d(t)$ and $r_m(t)$, taken together, give an indication of the changing strength of the wind velocity that the turbine experiences through the storm.

The next panels in Fig. 4(b) shows the yaw misalignment angle time series; the simulated wind velocity normal to the rotor plane at hub height, U_{norm}; the time-varying blade pitch angle; and the variation with time of the flapwise bending moment at a blade root. Between $t = 0$ s and $t = 200$ s, i.e., before the storm's intensity is felt at the turbine, the mean wind speed at hub height ($z = 90$ m) is approximately 6 m/s, which is below the rated wind speed (11.4 m/s) for this turbine. At these low winds, the blade pitch angle is zero and the power generated is less than the rated 5 MW level. As the storm picks up in intensity, the wind speed increases and the flapwise bending moment increases as well, while the blade pitch angle remains at zero until the rated wind speed is reached. At the rated wind speed, i.e., at $t \approx 260$ s, a first peak (or kink) in the flapwise bending moment time series is seen. Since the winds are continuing to increase, the blade pitch angle must increase in order to maintain the rated power of 5 MW and to limit structural loads (see Fig. 2). Higher wind speeds would be expected to increase loads on the blades; however, the increase in blade pitch angle decreases the blade loads at a faster rate and leads to a decreasing flapwise bending moment starting at $t \approx 260$ s. *It is the change in blade pitch angle from/to a zero value that produces the kink in the response time series.* As the winds get larger, the blade pitch angle continues to increase and the flapwise bending moment continues to decrease. As the winds begin to decrease after $t = 480$ s, the blade pitch angle decreases and the flapwise bending moment starts to pick up. At $t \approx 700$ s, the blade pitch angle goes to zero while the winds keep decreasing; then, flapwise loads also begin to decrease (this explains the second peak or kink in the flapwise bending moment time series).

B. Thunderstorm Risks to 6×4 Turbine Array

In the Monte Carlo simulations, for each set of "potential-impact" touchdown and track information, a job script executes FAST to loop over 6×4 wind turbines to simulate corresponding response. Each FAST output is post-processed to extract extreme wind speed and extreme flapwise bending moment of the three blades in the corresponding simulation. In order to isolate the influence of the storms' characteristics (i.e the non-turbulent part) on wind farm extreme loads, it is a good idea not to include the turbulence part, which is random, in FAST calculation. After a critical scenario is identified, turbulent wind field can be added later if a closer examination of the time series results is required.

Figure 5 shows the distribution of the wind farm average of extreme wind speed and extreme flapwise bending moment at a blade root resulting from 1,000 simulations for the JAWS Average and NIMROD Yorkville non-turbulent downbursts; the root of each arrow indicates the touchdown location of the simulated downburst while the direction of each arrow indicates the translation direction of the storm in the associated turbine response simulation. The color of the arrows gives an indication of the magnitude the corresponding wind farm average of extreme wind speed or extreme blade flapwise bending moment. As shown in Fig. 5, if the touchdown is close to the center of the farm but the storm is not fully developed then, low winds/loads result (shown as blue arrows in the plot). Low load (blue) cases where $x_0 > 0$ were already filtered out and are not shown in the figures. Red arrows indicate cases where the downburst arrives at the turbine at close to its fully developed state; maximum winds/loads are produced in these scenarios. The plot reveals touchdown locations and associated translational direction that are critical to wind farm extreme wind/load average. Note that the center of the wind farm is at $(x = 0, y = 0)$ on the plot. It appears that, in these particular cases, a storm that hits the ground in a 90-degree sector centered symmetrically relative to the X-direction in the wind farm's upwind area and that moves toward to the farm center causes large extreme winds/loads. Figure 5 also reveals that the NIMROD Yorkville downburst has quite different inflow characteristics than the JAW Average downburst, hence different load uncertainty features. It has both a larger maximum radial velocity (31 m/s) as well as a two times faster translation speed (16 m/s). Furthermore, the ambient wind speed is 8 m/s at hub height (compared to 6 m/s as in JAWS Average downburst) which is closer to rated wind speed (11.4 m/s). As a result, the NIMROD Yorkville downburst influences a larger area and creates higher chances of producing high winds and large loads at turbine units.

Figures 6 show the worst case (highest average load) resulting from 1000 scenarios for the JAWS Average. The small color-filled circles in the figure on the left, i.e. Figs. 6(a), represent the location of turbine units; color of these circles indicate the extreme flapwise bending moment at a blade root occurring during the non-turbulent downburst. The storm moves along the straight storm track, which is represented by the blue dash line. The three big circles along the track represent the storm location at touchdown (i.e. at $t = 0$), at maximum intensity (i.e. at $t = t_d/2 = 480$ s) and at the end of the event (i.e. at $t = t_d = 960$ s). The worst scenario results from at touchdown location and track direction that brings the storm to the wind farm at the storm's peak intensity and almost through the center of the farm. As a result, most of the turbine units are affected by this specific storm's movement, except the two units at each transverse-direction corners. The

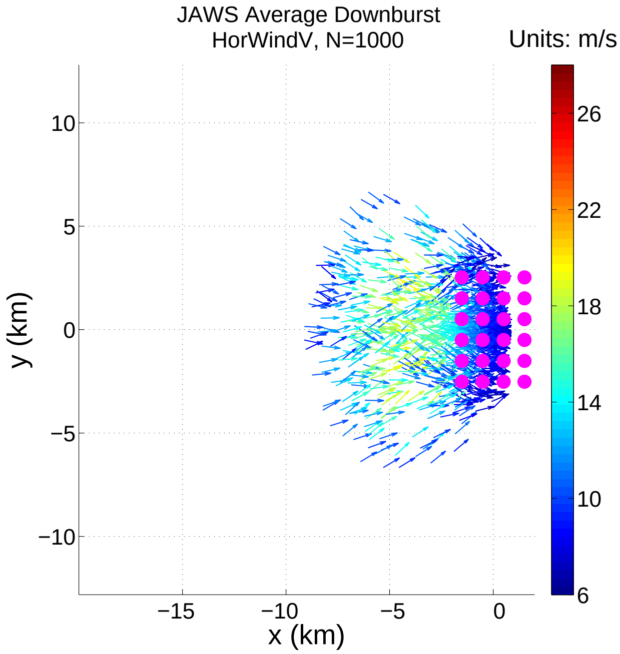

(a) Distribution of the Wind Farm Average of Extreme Wind at Hub Height from 1000 simulation for the JAWS Average Downburst

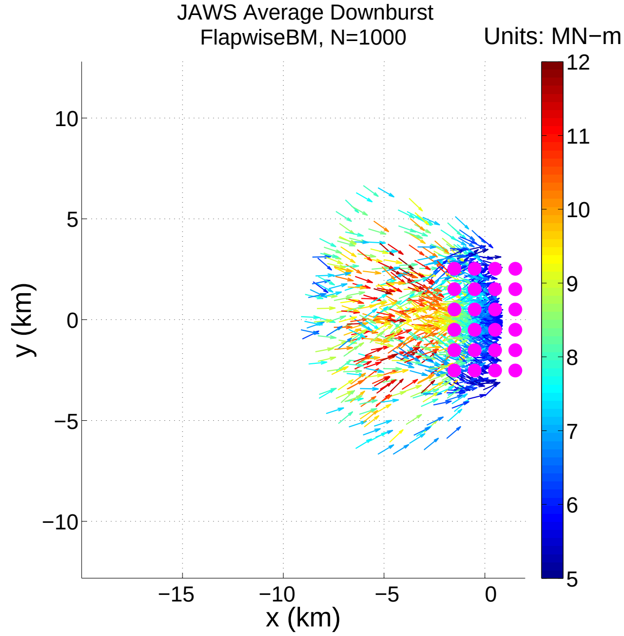

(b) Distribution of the Wind Farm Average of Extreme Flapwise Bending Moment at Blade Roots from 1000 simulation for the JAWS Average Downburst

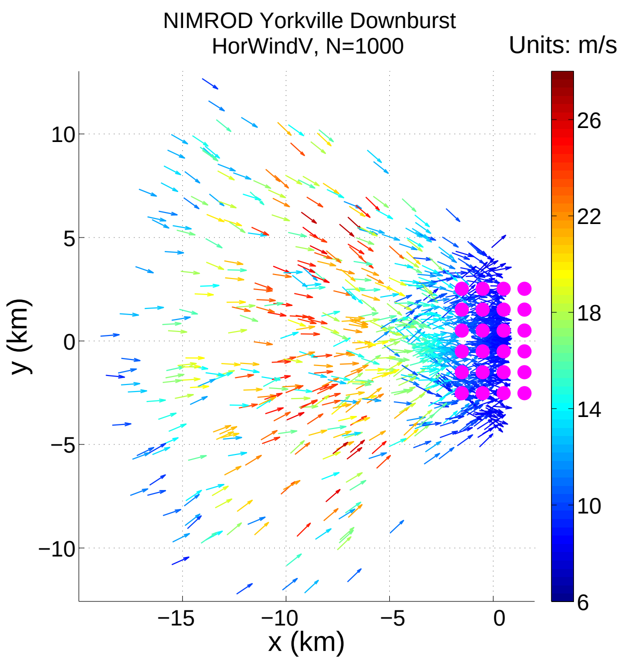

(c) Distribution of the Wind Farm Average of Extreme Wind at Hub Height from 1000 simulation for the NIMROD Yorkville Downburst

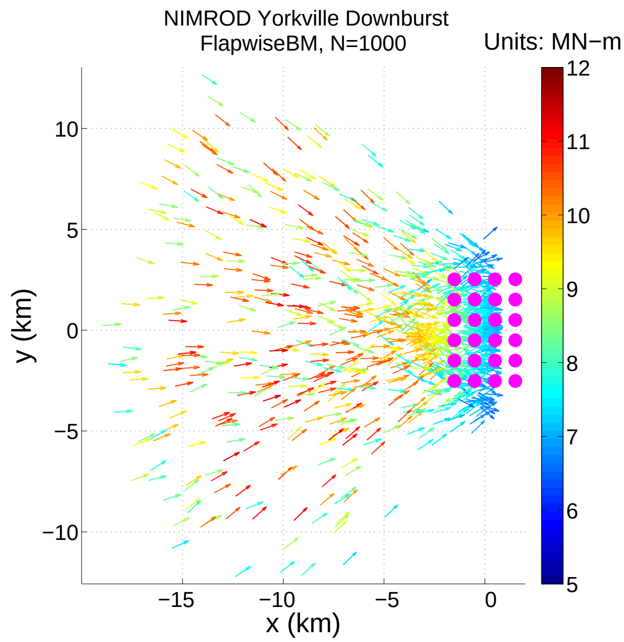

(d) Distribution of the Wind Farm Average Extreme Flapwise Bending Moment at Blade Roots from 1000 simulation for the NIMROD Yorkville Downburst

Figure 5. Distribution of the Wind Farm Average of Extreme Wind at Hub Height and Extreme Flapwise Bending Moment at Blade Roots accounting for Uncertainty in Storm Touchdown Location and Translation Direction.

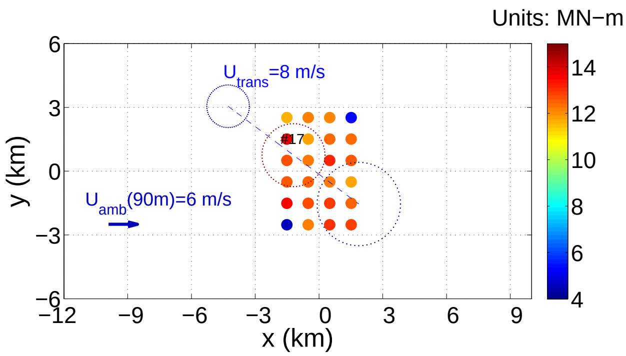

(a) Storm Track and Extreme Flapwise Bending Moment at Blade Roots due to Non-turbulent Downburst

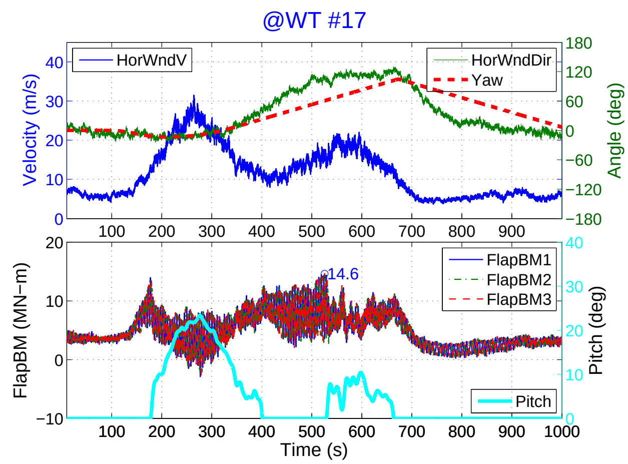

(b) Turbulent Wind Field, Yaw Control, Pitch Angle and Flapwise Bending Moment at Blade Roots Time Histories at Turbine #17 shown in Fig. 6(a).

Figure 6. The worst case out of 1000 Scenarios for JAWS Average Downburst where R_0 = 5.263 km; θ_0 = 144.5 deg.; ϕ = -36.8 deg. Note that U_{trans} = storm's translational speed; $U_{amb}(90m)$ = ambient wind velocity at 90 meters; $HorWndV$ = horizontal wind velocity at hub; $HorWndDir$ = horizontal wind direction at hub; Yaw = Yaw position of turbine's nacelle; $FlapBM1$ = flapwise bending moment at blade 1 root; $Pitch$ = blade pitch angle.

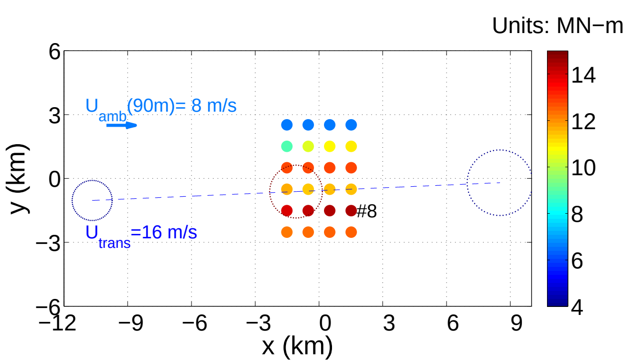

(a) Storm Track and Extreme Flapwise Bending Moment at Blade Roots due to Non-turbulent Downburst

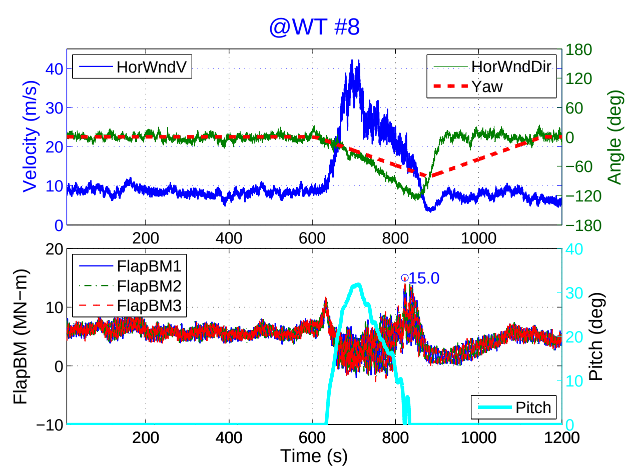

(b) Turbulent Wind Field, Yaw Control, Pitch Angle and Flapwise Bending Moment at Blade Roots Time Histories at Turbine #8 in Fig. 7(a).

Figure 7. The worst case out of 1000 Scenarios for the NIMROD Yorkville Case with R_0 = 10.737 km; θ_0 = 185.5 deg.; ϕ = 2.5 deg. Note that U_{trans} = storm's translational speed; $U_{amb}(90m)$ = ambient wind velocity at 90 meters; $HorWndV$ = horizontal wind velocity at hub; $HorWndDir$ = horizontal wind direction at hub; Yaw = Yaw position of turbine's nacelle; $FlapBM1$ = flapwise bending moment at blade 1 root; $Pitch$ = blade pitch angle.

extreme load at these two "trivial" units results from the ambient winds which is 6 m/s at hub. The highest extreme load occurs at turbine unit #17, see Fig. 6(a). Figure 6(b) shows the time histories of at turbine unit #17 whose both non-turbulent and turbulent parts are included in the simulation. There are two peaks in hub-height horizontal wind time history, one at $t = 260$ s and a smaller at $t = 560$ s, approximately. This "two-peak" characteristic of downbursts is often reported in measurements, for example Fujita,[19] Orwig and Schroeder.[6] There are four times when the blade pitch angle goes to zero, at t=180, 400, 525, 660 s, approximately; hence four "kinks" in load response. It is the change in blade pitch angle from a zero value that produces the kink in the response time series as discussed in Section A. Note that the highest peak, 14.6 MN-m, occurring at $t = 560$ s is associated with large yaw error.

The situation with simulations of the NIMROD Yorkville downburst is quite different from that with the JAWS downbursts. Although the Yorkville downburst moves faster (16 m/s) and has higher larger maximum radial velocity (31 m/s), its horizontal extent is smaller than that of the JAWS Average downburst. Its radial distance to maximum, $r_m(t)$, starts smaller ($r_{m0} = 940$ m) and increases slower ($k_{rm} = 0.5$ m/s) compared with the JAWS Average downburst ($r_{m0} = 1000$ m and $k_{rm} = 1$ m/s). Furthermore, the ambient wind speed is 8 m/s at hub height (compared to 6 m/s as in JAWS Average downburst) which is closer to rated wind speed (11.4 m/s). The fast storm translation speed ($U_{trans} = 16$ m/s) brings about a rapid change in wind velocity and wind direction which in turn causes fast wind velocity increase/decrease to/from rated wind speed and large yaw misalignment. These conditions are critical to wind turbine loads. The fast storm translation speed is an important characteristic of the downburst. As will be shown next, a fast moving downburst that moves in the same direction of the ambient wind can demand the highest capacity from a wind farm. Figure 7(a) shows the worst case (highest average load) that results from 1000 scenarios for the NIMROD Yorkville downburst. The track direction, $\phi = 2.5°$, is almost aligned with the ambient wind direction. Similar to the worst case of the JAWS Average downburst, the touchdown location and track direction brings the storm to the wind farm at the storm's peak intensity and near the center of the farm. In this case, the furthest turbine row from the storm track are not affected by the wind field created by storm movement. The extreme load at these units results from the ambient winds which 8 m/s at hub. The highest extreme load occurs at turbine unit #8, see Fig. 7(a). Figure 7(b) shows the time histories of this particular simulation whose wind field includes non-turbulent and turbulent parts. The two peaks in hub-height horizontal wind time history are not obvious. There are three times when the blade pitch angle goes to zero, at t=630, 810, 820 s, approximately; hence three "kinks" in load response. The last kink is caused mainly by turbulence fluctuations. Note that the largest peak, 15.0 MN-m, occurring at $t = 810$ s, is also associated with large yaw error.

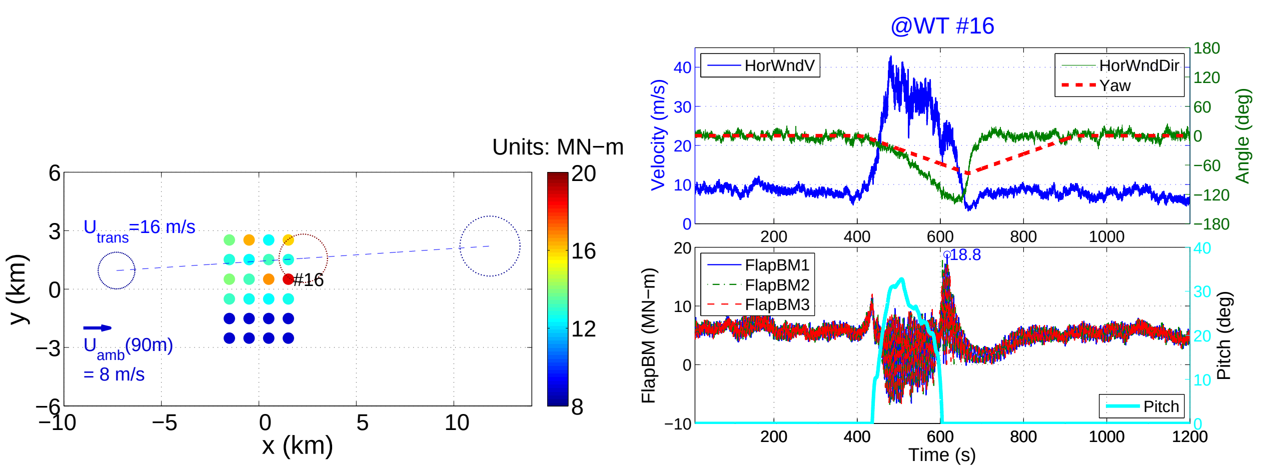

(a) Storm Track and Extreme Flapwise Bending Moment at Blade Roots due to Non-turbulent Downburst

(b) Turbulent Wind Field, Yaw Control, Pitch Angle and Flapwise Bending Moment at Blade Roots Time Histories at Turbine #16 in Fig. 8(a).

Figure 8. Simulation of Wind Fields and Turbine Loads for the NIMROD Yorkville Case with $R_0 = 7.379$ km; $\theta_0 = 172.6$ deg.; $\phi = 3.75$ deg. at the most critical unit. Note that U_{trans} = storm's translational speed; $U_{amb}(90m)$ = ambient wind velocity at 90 meters; $HorWndV$ = horizontal wind velocity at hub; $HorWndDir$ = horizontal wind direction at hub; Yaw = Yaw position of turbine's nacelle; $FlapBM1$ = flapwise bending moment at blade 1 root; $Pitch$ = blade pitch angle.

Of the two storms, the NIMROD Yorkville downburst is seen to be more critical to wind turbine loads. The fast storm translation speed (U_{trans} = 16 m/s) brings about a rapid change in wind velocity and wind direction. Although the NIMROD Yorkville storm lasts longer (20 minutes compared with 16 minutes as in JAWS Average), the duration of the transient felt at a wind turbine in the farm is shorter during NIMROD Yorkville downburst than in JAWS Average storm, as shown in Figs. 6(b) and 7(b). During such a short transient period, in addition to high wind speeds, the rate of wind direction change and the rate of wind speed change are both very high, pitch and yaw control even together are more likely insufficient to reduce turbine load range. Figure 8(b) shows the worst case (the highest single-turbine load) out of 1000 scenarios $\times$ 24 turbine units of the array or 24000 FAST simulations for the NIMROD Yorkville downburst which results from the scenario shown in Fig. 8(a). It is interesting to note that this scenario is somewhat similar to worst scenario (highest average load) of the NIMROD Yorkville downburst shown in Fig. 7(a) except that the storm is not fully developed when it comes to the farm and the offset distance from the center of the farm to the storm track is larger. These two factors do not make this scenario a critical case to the wind farm but to a single unit, i.e. turbine #16. Figure 8(b) shows the time histories of turbine #16 simulation in which wind field includes both non-turbulent and turbulent parts. One can see similar response to the case of Turbine #8 shown in Fig. 7(b). Note that the largest peak, 18.8 MN-m, occurring around $t = 605$ s, is roughly 4% higher than the 50-year load of IEC Design Load Case 1.1[20] as reported by Barone et al.[16]

VIII. Concluding Remarks

A wind field model for the simulation of thunderstorm downbursts was presented; non-turbulent and turbulent components of the field are generated separately. Two recorded downbursts, based on available information, were selected for a study of loads on an array of 6×4 five megawatt wind turbines. The storm's touchdown location and track direction with respect to the turbine array were modeled as random variables. Ambient wind direction was assumed to be normal to the longer side of the farm. With the use of high-performance computing resources, thousands of scenarios were simulated. Different downbursts have different characteristics, hence variable load uncertainty features to a wind farm. Results indicate that the demand capacity of a wind farm is high if a storm that hits the ground in a 90-degree sector centered symmetrically relative to the x-direction in the wind farm's upwind area and that moves toward to the farm location. For both downburst cases studied, the worst scenario results from a touchdown location and track direction that brings the storm to the wind farm at the storm's peak intensity and almost through the center of the farm. However, for the JAWS Average downburst, the translation direction is close to 45 degree with respect to the ambient wind direction while that of the NIMROD Yorkville downburst is almost aligned with the ambient wind direction. Other scenarios, e.g. one in which storm hits the ground near the farm center but then moves away, are not critical. In worst scenarios, extreme load on a wind turbine during a downburst can exceed 50-year load in normal operation conditions. The study highlights the need for enhancements to models for aerodynamic loads computation that can more accurately address large yaw error, yaw control, blade pitch control which were assumed in this paper.

ACKNOWLEDGEMENTS

The first two authors are pleased to acknowledge the financial support received from Sandia National Laboratories by way of Contract No. 743358. They are grateful too to Dr. Jason Jonkman of the National Renewable Energy Laboratory for continued assistance with FAST and with the turbine model. The use of the Sandia's E-Bird HPC system is also acknowledged.

References

[1] Nguyen, H. and Manuel, L., "A Monte Carlo Simulation Study of Wind Turbine Loads in Thunderstorm Downbursts," *52st AIAA/ASME/ASCE/AHS/ASC Structures, Structural Dynamics, and Materials Conference*, Denver, CO, 2011.

[2] Oseguera, R. and Bowles, R., "A Simple, Analytic 3-dimensional Downburst Model Based on Boundary Layer Stagnation Flow," Tech. Rep. NASATM-100632, NASA Langley Research Center, Hampton, VA, 1988.

[3] Vicroy, D., "A Simple, Analytical, Axisymmetric Microburst Model for Downdraft Estimation," Tech. Rep. NASATM-100632, NASA Langley Research Center, Hampton, VA, 1988.

[4] Chay, M., Albermani, F., and Wilson, R., "Numerical and Analytical Simulation of Downburst Wind Loads," *Engineering Structures*, Vol. 28, 2006, pp. 240–254.

[5] Kwon, D. and Kareem, A., "Gust-Front Factor: New Framework for Wind Load Effects on Structures," *JOURNAL OF STRUCTURAL ENGINEERING*, Vol. 135, 2009, pp. 717–732.

[6] Orwig, K. and Schroeder, J., "Near-surface Wind Characteristics of Extreme Thunderstorm Outflows," *Journal of Wind Engineering and Industrial Aerodynamics*, Vol. 95, 2007, pp. 565–584.

[7] Gast, K., *A Comparison of Extreme Wind Events as Sampled in the 2002 Thunderstorm Outflow Experiment*, M.S. Thesis, Texas Tech University, 2003.

[8] Orwig, K., *Examining Strong Winds from a Time-Varying Perspective*, Ph.D. Dissertation, Texas Tech University, 2010.

[9] Chen, L. and Letchford, C., "A Deterministic-Stochastic Hybrid Model of Downbursts and its Impact on a Cantilever Structure," *Engineering Structures*, Vol. 26, 2004, pp. 619–645.

[10] Fujita, T., "The Downburst: Microburst and Macroburst," Tech. Rep. NTIS PB-148880, Sattellite and Mesometeorology Research Project (SMRP) Research Paper 210, Dept. of Geophysical Sciences, Univ. of Chicago, Chicago (IL), 1985.

[11] Hjelmfelt, M., "Structure and Life Cycle of Microburst Outflows Observed in Colorado," *Journal of Applied Meteorology*, Vol. 27, 1988, pp. 900–927.

[12] Jonkman, J., Butterfield, S., Musial, W., and Scott, G., "Definition of a 5MW Reference Wind Turbine for Offshore System Development," Tech. Rep. NREL/TP-500-38060, National Renewable Energy Laboratory, Golden, CO, 2009.

[13] Veers, P., "Three-dimensional Wind Simulation," Tech. Rep. SAND88-0152, Sandia National Laboratory, Albuquerque, NM, 1988.

[14] Jonkman, J. and Buhl, M., "FAST User's Guide," Tech. Rep. NREL/EL-500-38230, National Renewable Energy Laboratory, Golden, CO, 2005.

[15] Jonkman, B., "TurbSim User's Guide: Version 1.50," Tech. Rep. NREL/TP-500-46198, National Renewable Energy Laboratory, Golden, CO, 2009.

[16] Barone, M., Paquette, J., Resor, B., and Manuel, L., "Decades of Wind Turbine Load Simulation," *50th AIAA Aerospace Sciences Meeting*, Nashville, TN, 2012.

[17] Adams, B., Bohnhoff, W., Dalbey, K., Eddy, J., Eldred, M., Gay, D., Haskell, K., Hough, P., , and Swiler, L., "DAKOTA, a multilevel parallel object-oriented framework for design optimization, parameter estimation, uncertainty quantification, and sensitivity analysis: Version 5.0 user's manual," Tech. Rep. Sandia Technical Report SAND2010-2183, Sandia National Laboratories, Albuquerque, NM, December 2009.

[18] McKay, M., Beckman, R., and Conover, W., "A Comparison of Three Methods for Selecting Values of Input Variables in the Analysis of Output from a Computer Code," *Technometrics*, Vol. 21(2), 1979, pp. 239–245.

[19] Fujita, T., "Andrews AFB Microburst," Tech. Rep. SMRP-205, University of Chicago, Chicago (IL), 1983.

[20] International Electrotechnical Commission, Wind Turbines - Part 1: Design Requirements, IEC-61400-1, Edition 3.0, 2007.